COMMUNICATIONS IN COMPUTATIONAL PHYSICS
Vol. **3**, No. 4, pp. 794-821

Commun. Comput. Phys.
April 2008

Numerical Simulation of Fluid Membranes in Two-Dimensional Space

Peng Song*, Dan Hu and Pingwen Zhang

LMAM and School of Mathematical Sciences, Peking University, Beijing 100871, China.

Received 17 May 2007; Accepted (in revised version) 9 October 2007

Available online 11 December 2007

Abstract. The membrane's dynamics is very important for cells. A membrane in 2-dimensional space can be seen as an incompressible closed curve in a plane or a cylindrical surface in 3-dimensional space. In this paper, we design a second-order accurate numerical algorithm to simulate the shape transformation of the membrane. In the algorithm, we use the tangent angles to present the curve and avoid the difficulties from the constraint of curve's incompressible condition. A lot of interesting phenomena are obtained. Some of them are very like the life processes of cells, such as exocytosis and endocytosis. Furthermore, we can see the relation between two dynamic models clearly. At last, considering the influence of the inner incompressible fluids partially, we add a constraint: the area circled by the membrane maintain invariable. The numerical results show the dynamic motions of a curve remaining its local arc length and inner area constant.

AMS subject classifications: 65M06, 65M12, 92C17

Key words: Director model of the membrane, reduced model, osmotic pressure, spontaneous curvature, constraint of the area.

1 Introduction

The membrane is probably the most important component in the cell. It surrounds all living cells and their organelles to maintain the cell's shape and regulate transport in and out of cells or subcellular domains. It also plays major role in many vital actions of cells, such as segmentation.

Recently, there has been a lot of experimental and analytic research on the configuration and deformation of elastic bio-membranes. In nature, a membrane consists chiefly

*Corresponding author. *Email addresses:* kevinsongpeng@yahoo.com.cn (P. Song), hudan@cims.nyu.edu (D. Hu), pzhang@pku.edu.cn (P. W. Zhang)

of lipids, proteins and carbohydrates. The structures and properties of membranes are very complex. One common method to simplify the structural analysis is to consider the membrane bilayers formed by certain amphiphilic molecules dissolved in water. In 1973, Helfrich [2] recognized that this lipid bilayer has the structure of a smectic liquid crystal. Based on the elastic theory of liquid crystals, he discovered the curvature elasticity model

$$E_H = \int_\Gamma (a + b(H - c_0) + cG)^2 \, ds,$$

where a is the surface tension, b,c are the bending rigidities and c_0 is the spontaneous curvature which describes the asymmetry effect of the membrane or the environment. A lot of work has been done in modeling the membrane using the theories for elastic shells. Steigmann [5, 6] considered the fluid films with curvature elasticity without viscous effects. Waxman [7–9] developed a kinetic model of the fluid dynamics on an evolving surface. Cai and Lubensky [10] derived a system of hydrodynamical equations for a fluid membrane and considered the renormalization of the compressibility and the dissipative coefficients. Pozrikidis [11–16] developed Waxman's model [9]. He considered the membrane as a compressible shell with bending resistance. Miao and his copartners [26–28] presented a general and systematic theory of non-equilibrium dynamics of multi-component fluid membranes. Hu et al. [1] developed an elastic energy model based on the Frank energy of the smectic liquid crystal by introducing the director field. The energy of the lipid directors balances the tendency to point parallel with neighbors and the normal vectors of the surface. If all the directors are constrained artificially on the direction of normal vectors, the energy will be reduced to Helfrich's curvature elastic energy as shown above. When the elastic coefficient in the director model tends to infinity, they obtained a reduced model. This reduced model is very like Waxman's model [9], but adds one term to the in-plane stresses, so that the model satisfy the second law of thermodynamics.

During the past several decades, a lot of numerical simulations have been performed so far. In 1976, Deuling and Helfrich [3] explained the characteristic bi-concave disk-like shape of the resting red blood cell, and obtained a rich catalog of axis-symmetric vesicle shapes with spontaneous curvature by the curvature elastic energy. In 1989, Svetina and Zeks [17] combined the bending elasticity with the bilayer-coupling hypotheses which leads to an additional constraint. They investigated part of the corresponding phase diagram of the equilibrium states. In 1991, Seifert et al. [19] systematically studied axisymmetric shapes which minimize the bending energy and determined the phase diagram for both the spontaneous-curvature and the bilayer-coupling models. They found a new branch of shapes, pear-shaped vesicles, and spheres connected by narrow necks. The occurrence of these shapes is intimately related to the budding phenomenon. In 2002, Capovilla [18] discussed the use of the stress tensor as a basis for perturbation theory and derived the first integral of the shape equation for axisymmetric configurations by examining the forces which are balanced along the circles of constant latitude. In 2004, Gerald and Michael [20] used continuum mechanics to model the red blood cell's membrane

and numerically simulated the shapes and the stomatocyte-discocyte-echinocyte shape transformations. Du et al. [21, 22] used a variational energetic phase field model based on Helfrich's curvature elastic energy [2] to compute the equilibrium configurations of a membrane. They can get many configurations, particularly discocyte and stomatocyte types. In [24], using the similar method, they systematically analyzed the shape transformations of the vesicles in the real physical 3-dimensional space and explored the non-axisymmetric shapes and discovered new configurations. Furthermore, they considered how to use the Euler number to detect topological change in the membrane deformation.

All the numerical methods can be sorted into two classes. One is to employ a mesh on the membrane, which can be seen as an evolving interface, and track its motion, such as the boundary integral methods, boundary element methods [38, 39]. This kind of methods can show the interface's exact position and local dynamics in detail. Another class of methods is to write a system of equations on the entire domain by representing the tension of the interface as a body force over a narrow region which covers the interface. A fixed grid can be employed in the Eulerian framework, such as the level-set method [40–42], the front-tracking method [43,44], the phase field method [22–24]. These methods can avoid the mesh entanglement which is a difficulty for the first kind of methods. But they cannot describe the local dynamic characterization of the interface in detail exactly. Our method belongs to the first class. We employ a regular grid on the membrane and disperse the equations of the director model. By the numerical computing, we can keep tracking the motion of the membrane. This method can describe the membrane's position and dynamic properties exactly, particularly the directors on the membrane.

In this paper, we describe three contributions. First, we employ numerical methods to simulate the dynamics of a moving membrane in 2-dimensional space using the director model. The membrane in 2-dimensional space is a closed curve with a director field on it, which also can be seen as a cylindrical surface in 3-dimensional space. We study its dynamical processes effected by the spontaneous-curvature or osmotic pressure. We can see that the exocytosis and endocytosis can be explained by local spontaneous curvature.

Another contribution of this paper is on the relation between the director model and the reduced model. In [1], Hu et al. formally attained the reduced model by the limiting case of the director model. In this paper, we can see it clearly from the numerical results.

Finally, we study the membrane's motion in 2-dimensional space with a constraint: the area circled by the curve remains constant. In fact, the membrane is immersed in some incompressible fluids. Thus, its inner area is constrained by the fluids. Considering the influence of the incompressible fluids practically, we add the area constraint to the curve artificially in order to study the dynamics of a curve remaining its local arc length and inner area invariable.

The rest of the paper is organized as follows. In Section 2, we introduce the director model and the reduced model in detail and reduce them in 2-dimensional space. In Section 3, we outline the numerical algorithms for simulating the director model. In Section 4, we present the diagrams for the simulation results, discuss in detail the various solution branches and study the relation between the director model and the reduced

model. In Section 5, we consider the area-constrained situation and lay out the numerical results. In Section 6, we make some concluding remarks.

2 Introduction to two dynamical models

2.1 The director model

In this section, we introduce the director model. In [1], Hu et al. assume the membrane composed of rodlike molecules is a Cosserat surface with a director field on it. We use Γ to express the surface. On Γ, they introduced Lagrangian coordinates $u^\alpha(\alpha=1,2)$, and the position of the surface in Euclidean space is $\mathbf{R}(u^\alpha,t)$. The Frenet coordinate system of the surface – the tangent vectors $\mathbf{a}_\alpha$ and the unit normal vector $\mathbf{n}$ are

$$\mathbf{a}_\alpha=\frac{\partial \mathbf{R}}{\partial u^\alpha}, \tag{2.1}$$

$$\mathbf{n}\cdot\mathbf{a}_\alpha=0, \quad \mathbf{n}\cdot\mathbf{n}=1. \tag{2.2}$$

Then the metric tensor $a_{\alpha\beta}$, the covariant alternating tensor $\varepsilon_{\alpha\beta}$, and the curvature tensor $b_{\alpha\beta}$ can also be given. The unit director field is $\mathbf{O}$. To describe the motion of the surface, they also introduce the velocity of the surface

$$\mathbf{v}(u^\alpha,t)=\frac{\partial \mathbf{R}}{\partial t}, \tag{2.3}$$

which has a decomposition

$$\mathbf{v}=v^\alpha\mathbf{a}_\alpha+v^{(n)}\mathbf{n}.$$

Here, the superscript α of v^α means the decomposition of $\mathbf{v}$ along the tangent vector $\mathbf{a}_\alpha$:

$$v^\alpha=\mathbf{v}\cdot\mathbf{a}_\alpha,$$

and the superscript (n) of $v^{(n)}$ means the decomposition along the unit normal vector $\mathbf{n}$:

$$v^{(n)}=\mathbf{v}\cdot\mathbf{n}.$$

The same applies to other vectors. The relationships among the physical quantities are all described in detail in [1]. We do not repeat them here.

Basing on the Frank energy for liquid crystals, D.Hu etc. discovered the elastic energy of the director field,

$$\begin{aligned} E_{el} = & \frac{k_2}{2}O^\alpha O_\alpha+\frac{k_1+\varepsilon_1}{2}a^{\alpha\beta}(\mathbf{O}_{,\alpha}+\mathbf{b}_\alpha)\cdot(\mathbf{O}_{,\beta}+\mathbf{b}_\beta) \\ & +\frac{k_1-\varepsilon_1}{2}\varepsilon^{\alpha\beta}((\mathbf{O}_{,\alpha}+\mathbf{b}_\alpha)\times(\mathbf{O}_{,\beta}+\mathbf{b}_\beta))\cdot\mathbf{O}, \end{aligned} \tag{2.4}$$

where k_1,k_2 and ε_1 are positive elastic coefficient and $k_1\geq\varepsilon_1$; $\mathbf{b}_\alpha$ is the spontaneous curvature. The spontaneous curvature is important for the shape of a membrane. In

the 2-dimensional space, it must be vertical to the director $\mathbf{O}$ and independent of time. The comma followed by a lowercase Greek subscript, such as $\mathbf{O}_{,\alpha}$, denotes the covariant derivative based on the metric tensor $a_{\alpha\beta}$. By applying the principle of virtual work, the torque and stress induced by the director field were determined. The dynamical equations of the director model are obtained by applying the conservation laws for the linear and angular momentum. The following is the model equations in 3-dimensional space:

$$\gamma\frac{\partial \mathbf{v}}{\partial t}=\mathbf{f}+\left(T^{\alpha\beta}\mathbf{a}_\beta\right)_{,\alpha}+k_2\left(O^{(n)}O^\alpha\mathbf{n}\right)_{,\alpha}, \tag{2.5}$$

$$\gamma\phi\mathbf{O}\times\frac{\partial^2\mathbf{O}}{\partial t^2}=(k_1+\varepsilon_1)a^{\alpha\beta}\mathbf{O}\times(\mathbf{O}_{,\alpha}+\mathbf{b}_\alpha)_{,\beta}+(k_1-\varepsilon_1)\varepsilon^{\alpha\beta}\mathbf{O}\times\left(\mathbf{O}\times\mathbf{b}_{\alpha,\beta}\right) -k_2O^\alpha\mathbf{O}\times\mathbf{a}_\alpha, \tag{2.6}$$

$$v^\alpha_{,\alpha}-2Hv^{(n)}=0, \tag{2.7}$$

where γ is the density of the molecules, ϕ is the length of the molecule, $\mathbf{f}$ is the extra forces (which will be taken as the osmotic force $f_{osm}\mathbf{n}$ in Section 3 or the force to keep the area constant in Section 5.1), and H is the mean curvature. The last equation is the incompressible condition of the surface which means any local area of the surface keeps constant. For isotropic fluids, the surface stress tensor $T^{\alpha\beta}$ is

$$T^{\alpha\beta}=-\Pi a^{\alpha\beta}+J^{\alpha\beta}+(k_1+\varepsilon_1)a^{\alpha\gamma}a^{\beta\delta}O_{,\gamma}\cdot O_{,\delta}, \tag{2.8}$$

$$J^{\alpha\beta}=C^{\alpha\beta\gamma\delta}S_{\gamma\delta}, \tag{2.9}$$

$$C^{\alpha\beta\gamma\delta}=(k_0-\varepsilon_0)a^{\alpha\beta}a^{\gamma\delta}+\varepsilon_0\left(a^{\alpha\gamma}a^{\beta\delta}+a^{\alpha\delta}a^{\beta\gamma}\right). \tag{2.10}$$

Without the extra force $\mathbf{f}$, we have an energy estimation

$$\frac{\partial}{\partial t}\int_\Gamma\left(\frac{\gamma}{2}|\mathbf{v}|^2+\frac{\gamma\phi}{2}\left|\mathbf{O}\times\frac{\partial\mathbf{O}}{\partial t}\right|^2+E_{el}\right)dS=-2\varepsilon_0\int_\Gamma S^{\alpha\beta}S_{\alpha\beta}\,dS, \tag{2.11}$$

where

$$S_{\alpha\beta}=\frac{1}{2}(v_{\alpha,\beta}+v_{\beta,\alpha})-v^{(n)}b_{\alpha\beta}$$

is the rate of strain.

2.2 The reduced model

The reduced model is obtained by $k_2\to+\infty$. While k_2 gets larger and larger, in the elastic energy E_{el}, the term $\frac{1}{2}k_2O^\alpha O_\alpha$ will be larger as well if the amplitudes of directors' vibrations remain constant. To get the lowest energy, O^1 must be smaller. It means the directors can not wag too much away from the normal direction. The directors oscillate with such a large frequency that the effect of the directors will be average determined by their equilibrium positions. Thus there is no equation for directors any longer. The

in-plane stress $T^{\alpha\beta}$ and the transverse shear stress $k_2 O^\alpha O_\alpha$ are all changed. Based on this idea, they obtained the ultimate equations as $k_2 \to +\infty$:

$$\gamma \frac{\partial \mathbf{v}}{\partial t} = \mathbf{f} + \left(T^{\alpha\beta} \mathbf{a}_\beta \right)_{,\alpha} + \left(q^\alpha \mathbf{n} \right)_{,\alpha}, \tag{2.12}$$

$$v^\alpha_{,\alpha} - 2Hv^{(n)} = 0, \tag{2.13}$$

where q^α is the ultimate transverse share stress,

$$q^\alpha = M^{\alpha\beta}_{,\beta}, \tag{2.14}$$

$$M^{\alpha\beta} = C^{\alpha\beta\gamma\delta} \left(B_{\gamma\delta} - b_{\gamma\delta} \right). \tag{2.15}$$

Here, the tensor $B_{\gamma\delta}$ is another expression of the spontaneous curvature

$$\mathbf{b}_\gamma = B_{\gamma\delta} a^{\delta\mu} \mathbf{a}_\mu. \tag{2.16}$$

The ultimate in-plane stress $T^{\alpha\beta}$ is

$$T^{\alpha\beta} = -\Pi a^{\alpha\beta} + J^{\alpha\beta} + M^{\alpha\mu} b^\beta_\mu. \tag{2.17}$$

In this model, there are only two variables left: $\mathbf{R}$ and Π. For this model, the energy estimation is

$$\frac{\partial}{\partial t} \int_\Gamma \left(\frac{\gamma}{2} |\mathbf{v}|^2 + E_{el} \right) ds = -2\varepsilon_0 \int_\Gamma S^{\alpha\beta} S_{\alpha\beta} \, ds, \tag{2.18}$$

where E_{el} is the elastic energy

$$E_{el} = C^{\alpha\beta\gamma\delta} \left(B_{\alpha\beta} - b_{\alpha\beta} \right) \left(B_{\gamma\delta} - b_{\gamma\delta} \right). \tag{2.19}$$

The director model and the reduced model all contain four parts: the elastic part, the viscous part, the visco-elastic response and the effect of the local spontaneous curvature. Many models before them always lacked something. For example, Waxman's model [9] missed an elastic in-plane stress term; Capovilla and Guven's model [18] neglects the viscous contributions; Lomholt and Miao's model [28] considered the mechanics of the membrane with bending energy, but not the dynamics. The director model and the reduced model can describe a lot of dynamic properties of the membrane, which is our motivation to simulate these two models numerically.

2.3 The equations in 2-dimensional space

A membrane in 2-dimensional space can be seen as an incompressible closed curve in a plane or a cylindrical surface in 3-dimensional space. In nature, there is no real 1-dimensional incompressible fluid. Thus, in fact, the 2-dimensional membrane is an incompressible elastic string with no viscosity. Derived from this description, the equations

of the director model in the 2-dimensional space are

$$\gamma\frac{\partial \mathbf{v}}{\partial t}=\frac{\partial(T\mathbf{a})}{\partial s}+k_2\frac{\partial(O^{(n)}O^1\mathbf{n})}{\partial s}+f_{osm}\mathbf{n}, \tag{2.20}$$

$$\gamma\phi\mathbf{O}\times\frac{\partial^2\mathbf{O}}{\partial t^2}=(k_1+\varepsilon_1)\mathbf{O}\times\frac{\partial}{\partial s}\left(\frac{\partial\mathbf{O}}{\partial s}+\mathbf{b}\right)-k_2O^1\mathbf{O}\times\mathbf{a}, \tag{2.21}$$

$$\frac{\partial v^1}{\partial s}-\kappa v^{(n)}=0, \tag{2.22}$$

where s is the arc length parameter of the closed curve, $\kappa=2H$ is the curvature, and the in-plan stress is reduced to a scalar T. Since in the 2-dimensional space the covariant alternating tensor $\varepsilon_{\alpha\beta}$ vanishes, the right part of Eq. (2.21) and the elastic energy E_{el} all have only two terms left. Here, we only consider the extra force $\mathbf{f}$ to be the osmotic force $f_{osm}\mathbf{n}$ which is along the normal vector.

The energy estimation is reduced to

$$\frac{\partial}{\partial t}\int_\Gamma\left(\frac{\gamma}{2}|\mathbf{v}|^2+\frac{\gamma\phi}{2}\left|\mathbf{O}\times\frac{\partial\mathbf{O}}{\partial t}\right|^2+E_{el}\right)dS=0,$$

where

$$E_{el}=\frac{k_2}{2}O^1O_1+\frac{k_1+\varepsilon_1}{2}(\frac{\partial\mathbf{O}}{\partial s}+\mathbf{b})\cdot(\frac{\partial\mathbf{O}}{\partial s}+\mathbf{b}).$$

The initial conditions of the system of Eqs. (2.20)-(2.22) are

$$\mathbf{R}(s,t)|_{t=0}=\mathbf{R}^0(s),\quad \mathbf{O}(s,t)|_{t=0}=\mathbf{O}^0(s),$$
$$\mathbf{v}(s,t)|_{t=0}=\mathbf{v}^0(s),\quad \left.\frac{\partial\mathbf{O}(s,t)}{\partial t}\right|_{t=0}=\mathbf{O}_t^0(s),$$

where the initial velocity $\mathbf{v}^0(s)$ must satisfy the incompressibility condition (2.22). The boundary condition is the periodic condition for the closed curve. This model is just like a closed evolving elastic string in a plane.

Similarly, the equations of the reduced model in 2-dimensional space are

$$\gamma\frac{\partial\mathbf{v}}{\partial t}=\frac{\partial(T\mathbf{a})}{\partial s}+\frac{\partial(q\mathbf{n})}{\partial s}+f_{osm}\mathbf{n}, \tag{2.23}$$

$$\frac{\partial v^1}{\partial s}-\kappa v^{(n)}=0. \tag{2.24}$$

The stresses T and $q=\varepsilon(B-\kappa)_s$ are all scalars. The reduced model is the same as Waxman's model in the elastic case [9]. The energy estimation is

$$\frac{\partial}{\partial t}\int_\Gamma\left(\frac{\gamma}{2}|\mathbf{v}|^2+E_{el}\right)ds=0,$$

where E_{el} is the elastic energy

$$E_{el}=\varepsilon(\kappa-B)^2.$$

It is the same as Helfrich's curvature elasticity energy.

2.4 The equations of tangent angles

Our primary goal is to solve the director model Eqs. (2.20)-(2.22) with initial and periodic boundary conditions. Then the reduced model (2.23) and (2.24) can be solved using the similar numerical methods. The director model is similar to a complicated motion-by-curvature problem. A method of using the arc length frame of reference to remove the stiffness from interfacial flows was introduced in [45–47]. In our problem, similarly, we need to deal with the difficulties caused by the nonlinear terms of curvature and the incompressible condition of the membrane. Thus we use the arc length frame of reference as well. Since the incompressible condition of the membrane in 2-dimensional space means the local arc length remains constant, the arc length coordinate will be always the Lagrangian coordinate. The position of the curve can be expressed by the tangent angles, the length of the curve and the position of curve's center of gravity. Additionally, the incompressible condition of the curve will be satisfied automatically by the unit tangent vectors.

There is another advantage using the tangent angle. In the system of Eqs. (2.20)-(2.22) curvature κ is a very important quantity. It is hard to approximate numerically with higher order accuracy from $\mathbf{R}$. But it is much easier to compute it with second-order accuracy from the tangent angle.

Let $s\in[0,L]$ be the arc length coordinate, $|\mathbf{a}|=1$. We can assume

$$\mathbf{a}=(\cos\alpha(s,t),\sin\alpha(s,t))$$

and the outside normal vector is

$$\mathbf{n}=(\sin\alpha(s,t),-\cos\alpha(s,t)),$$

where α is the angle between the curve's tangent vector and the positive direction of the x-axis. Similarly, we let the unit director $\mathbf{O}$ be expressed by another angle θ: $\mathbf{O}=(\cos\theta(s,t),\sin\theta(s,t))$. Its tangential and normal components are

$$O^1=\cos(\alpha-\theta),\quad O^{(n)}=\sin(\alpha-\theta).$$

The curvature $\kappa=-\partial\alpha/\partial s$ and the incompressible condition is satisfied naturally. By the equalities

$$\frac{\partial^2\mathbf{v}}{\partial t\partial s}\cdot\mathbf{n}=\frac{\partial^2\mathbf{a}}{\partial t^2}\cdot\mathbf{n}=-\frac{\partial^2\alpha}{\partial t^2},$$
$$\frac{\partial^2\mathbf{v}}{\partial t\partial s}\cdot\mathbf{a}=\frac{\partial^2\mathbf{a}}{\partial t^2}\cdot\mathbf{a}=-\left(\frac{\partial\alpha}{\partial t}\right)^2,$$

Eq. (2.20) is reduced to two equations of α,

$$\gamma\alpha_{tt}=2T_s\alpha_s+T\alpha_{ss}+\frac{1}{2}k_2\left[(\beta_s^2+\alpha_s^2)\sin\beta-\beta_{ss}\cos\beta\right], \tag{2.25}$$

$$-\gamma(\alpha_t)^2=T_{ss}-T(\alpha_s)^2+\frac{1}{2}k_2\left[2\beta_s\alpha_s\cos\beta+\alpha_{ss}\sin\beta\right]+f_{osm}\alpha_s, \tag{2.26}$$

where $\beta=2(\alpha-\theta)$ and the subscript t,s means the derivative of time and arc length parameter. Since the spontaneous curvature $\mathbf{b}$ is vertical to the director $\mathbf{O}$, it can be replaced by

$$\mathbf{b}=l(s)(-\sin\theta,\cos\theta),$$

where $l(s,t)$ is a scalar representing the length of $\mathbf{b}$. Eq. (2.21) is rewritten as an equation of θ as well

$$\gamma\phi\theta_{tt}=-k_2\cos(\alpha-\theta)\sin(\alpha-\theta)+k(\theta_{ss}+l_s), \tag{2.27}$$

where $k=k_1+\varepsilon_1$. The variables in these three equations are α,θ,T. Eq. (2.26) can be viewed as a constraint of α and T. If we know the angles α,θ and their velocities α_t,θ_t, the positions and velocities of curve and directors can be resolved by

$$\frac{\partial\mathbf{R}(s,t)}{\partial s}=\mathbf{a}(s,t),\quad \mathbf{O}(s,t)=(\cos\theta(s,t),\sin\theta(s,t)), \tag{2.28}$$

$$\frac{\partial\mathbf{v}(s,t)}{\partial s}=-\alpha_t\mathbf{n},\quad \mathbf{O}\times\frac{\partial\mathbf{O}}{\partial t}=\theta_t, \tag{2.29}$$

with the periodic boundary condition and the integral conditions

$$\int_\Gamma\mathbf{v}\,ds=\int_\Gamma\mathbf{v}_0\,ds,\quad \frac{\partial}{\partial t}\int_\Gamma\mathbf{R}\,ds=\int_\Gamma\mathbf{v}\,ds=\int_\Gamma\mathbf{v}_0\,ds.$$

These two integral equations tell us that the curve's gravity center moves in a constant velocity $\int_\Gamma\mathbf{v}_0\,ds$. In the numerical simulations, we always let the initial velocity $\mathbf{v}_0$ satisfy $\int_\Gamma\mathbf{v}_0\,ds=0$ to fix the gravity center. The initial conditions are changed into

$$\begin{aligned}&\alpha(s,0)=\alpha^0(s),\quad \theta(s,0)=\theta^0(s),\\ &\alpha_t(s,0)=\alpha_t^0(s),\quad \theta_t(s,0)=\theta_t^0(s).\end{aligned}$$

The initial data of angles can be obtained by

$$\begin{aligned}&(\cos\alpha^0,\sin\alpha^0)=\frac{\partial\mathbf{R}^0}{\partial s},\quad (\cos\theta^0,\sin\theta^0)=\mathbf{O}^0,\\ &\alpha_t^0=-\frac{\partial\mathbf{v}^0}{\partial s}\cdot\mathbf{n},\qquad\qquad \theta_t^0=\mathbf{O}\times\mathbf{O}_t^0.\end{aligned}$$

If $\mathbf{v}\equiv0$ and $\frac{\partial\mathbf{O}}{\partial t}=0$ in the director model without extra forces and spontaneous curvatures, we get the equations

$$2T_s\alpha_s+T\alpha_{ss}+\frac{1}{2}k_2\left[\beta_{ss}\cos\beta-(\beta_s^2+\alpha_s^2)\sin\beta\right]=0, \tag{2.30}$$

$$T_{ss}-T(\alpha_s)^2+\frac{1}{2}k_2\left[2\beta_s\alpha_s\cos\beta+\alpha_{ss}\sin\beta\right]=0, \tag{2.31}$$

$$-k_2\cos(\alpha-\theta)\sin(\alpha-\theta)+k\theta_{ss}=0. \tag{2.32}$$

It is easy to solve $\alpha = 2\pi s/L$, and $\theta = \alpha$ or $\theta = \alpha + \frac{\pi}{2}$. The solution $\theta = \alpha$ is unstable. Thus the steady state is a circle with director **O** parallel to the normal **n**.

The equations of the reduced model (2.23) and (2.24) can also be converted to angle form,

$$\gamma\alpha_{tt} = 2T_s\alpha_s + T\alpha_{ss} - \varepsilon\left[(B_s+\alpha_{ss})_{ss} - (B_s+\alpha_{ss})\alpha_s^2\right],$$
$$-\gamma(\alpha_t)^2 = T_{ss} - T(\alpha_s)^2 + \varepsilon\left[(B_s+\alpha_{ss})\alpha_{ss} + 2(B_s+\alpha_{ss})_s\alpha_s\right],$$

which are similar to the director model without the angle of directors θ.

3 Numerical method

We assume the length of the curve L to be 1 and take the division of the curve and time

$$0 = s_0 < s_1 < \cdots < s_{N-1} < s_N = 1,$$
$$s_i = i\Delta s = \frac{i}{N}, \quad i = 0,1,\cdots,N; \quad t_j = j\Delta t,$$

where Δt is the time step size. Let $\alpha_i^j = \alpha(s_i,t_j)$, which is the same as other variables. To assure higher accuracy of the discrete initial conditions, we introduce the time step $t_{-1} = -\Delta t$ and the corresponding physical quantities, such as

$$\alpha_i^{-1} = \alpha(s_i,t_{-1}).$$

Then we have the discrete initial conditions with the second-order accuracy

$$\alpha_i^0 = \alpha^0(s_i), \quad \frac{\alpha_i^1 - \alpha_i^{-1}}{2\Delta t} = \alpha_t^0(s_i), \tag{3.1}$$

$$\theta_i^0 = \theta^0(s_i), \quad \frac{\theta_i^1 - \theta_i^{-1}}{2\Delta t} = \theta_t^0(s_i). \tag{3.2}$$

Eqs. (2.25) and (2.27) look like wave equations for α, thus we use the central difference formulas on time and space. Here we show only the discrete formula of time. The discretizations on space all use the central difference formula.

$$\gamma\frac{\alpha_i^{j+1} - 2\alpha_i^j + \alpha_i^{j-1}}{\Delta t^2} = \left[2T_s\alpha_s + T\alpha_{ss} + \frac{1}{2}k_2\left[(\beta_s^2+\alpha_s^2)\sin\beta - \beta_{ss}\cos\beta\right]\right]_i^j, \tag{3.3}$$

$$\gamma\phi\frac{\theta_i^{j+1} - 2\theta_i^j + \theta_i^{j-1}}{\Delta t^2} = \left[-k_2\cos(\alpha-\theta)\sin(\alpha-\theta) + k(\theta_{ss}+l_s)\right]_i^j. \tag{3.4}$$

Eq. (2.26) is a constraint for α and T, which means α and T must satisfy this equation on each time step. Similarly, we can also use central difference formula.

$$-\gamma\left(\frac{\alpha_i^{j+1} - \alpha_i^{j-1}}{2\Delta t}\right)^2 = \left[T_{ss} - T(\alpha_s)^2 + \frac{1}{2}k_2\left[2\beta_s\alpha_s\cos\beta + \alpha_{ss}\sin\beta\right] + f_{osm}\alpha_s\right]_i^j. \tag{3.5}$$

By letting $j=0$, Eqs. (3.3), (3.5) and (3.4) become

$$\gamma\frac{\alpha_i^1-2\alpha_i^0+\alpha_i^{-1}}{\Delta t^2}=\left[2T_s\alpha_s+T\alpha_{ss}+\frac{1}{2}k_2\left[(\beta_s^2+\alpha_s^2)\sin\beta-\beta_{ss}\cos\beta\right]\right]_i^0, \tag{3.6}$$

$$-\gamma\left(\frac{\alpha_i^1-\alpha_i^{-1}}{2\Delta t}\right)^2=\left[T_{ss}-T(\alpha_s)^2+\frac{1}{2}k_2\left[2\beta_s\alpha_s\cos\beta+\alpha_{ss}\sin\beta\right]+f_{osm}\alpha_s\right]_i^0, \tag{3.7}$$

$$\gamma\phi\frac{\theta_i^1-2\theta_i^0+\theta_i^{-1}}{\Delta t^2}=\left[-k_2\cos(\alpha-\theta)\sin(\alpha-\theta)+k(\theta_{ss}+l_s)\right]_i^0. \tag{3.8}$$

Putting Eq. (3.1) into (3.7) gives a system of linear algebraic equation for T_i^0. Then the pressure T_i^0 can be solved. By the discrete initial conditions (3.1) and (3.2), the quantities at time t_{-1} can be expressed by the quantities at time t_0,t_1

$$\alpha_i^{-1}=\alpha_i^1-2\Delta t\alpha_t^0(s_i), \tag{3.9}$$

$$\theta_i^{-1}=\theta_i^1-2\Delta t\theta_t^0(s_i). \tag{3.10}$$

From Eqs. (3.6) and (3.8), we can get two equations; one is for α_i^1 only, another is for θ_i^1. Thus we obtain $T_i^0,\alpha_i^1,\alpha_i^0,\theta_i^1,\theta_i^0$.

Assuming we have the values of $T_i^{j-1},\alpha_i^j,\alpha_i^{j-1},\theta_i^j,\theta_i^{j-1}$, then θ_i^{j+1} can be easily solved by Eq. (3.5). Eqs. (3.3) and (3.5) depend upon α_i^{j+1} and T_i^j, but the second one is a nonlinear equation for α_i^{j+1}. We tried the nonlinear iteration method to solve this system of equations, but it is found not convergent. Trying to linearize Eq. (3.5), we introduce the "velocity" of the angle at the middle time $t_{j+\frac{1}{2}}=(j+\frac{1}{2})\Delta t$ as

$$(\alpha_t)_i^{j+\frac{1}{2}}=\frac{\alpha_i^{j+1}-\alpha_i^j}{\Delta t}.$$

Then Eqs. (3.3) and (3.5) can be expressed as

$$\gamma\frac{(\alpha_t)_i^{j+\frac{1}{2}}-(\alpha_t)_i^{j-\frac{1}{2}}}{\Delta t}=\left[2T_s\alpha_s+T\alpha_{ss}+\frac{1}{2}k_2\left[(\beta_s^2+\alpha_s^2)\sin\beta-\beta_{ss}\cos\beta\right]\right]_i^j, \tag{3.11}$$

$$-\gamma\left(\frac{(\alpha_t)_i^{j+\frac{1}{2}}+(\alpha_t)_i^{j-\frac{1}{2}}}{2}\right)^2=\left[-k_2\cos(\alpha-\theta)\sin(\alpha-\theta)+k(\theta_{ss}+l_s)\right]_i^j. \tag{3.12}$$

Considering the nonlinear part of $(\alpha_t)_i^{j+\frac{1}{2}}$

$$\left(\frac{(\alpha_t)_i^{j+\frac{1}{2}}+(\alpha_t)_i^{j-\frac{1}{2}}}{2}\right)^2$$

which is a second-order approximation of α_t^2, we use a linear approximation instead of

$$(\alpha_t)_i^{j+\frac{1}{2}}(\alpha_t)_i^{j-\frac{1}{2}}.$$

It has the same order of accuracy. Eq. (3.12) is changed into

$$-\gamma(\alpha_t)_i^{j+\frac{1}{2}}(\alpha_t)_i^{j-\frac{1}{2}}=[-k_2\cos(\alpha-\theta)\sin(\alpha-\theta)+k(\theta_{ss}+l_s)]_i^j. \tag{3.13}$$

Now, the system of Eqs. (3.11) and (3.13) is a closed linear system of variables $(\alpha_t)_i^{j+\frac{1}{2}}$ and T_i^j, which can be solved easily. Then by Eqs. (2.28) and (2.29), we can obtain $\mathbf{R}_i^{j+1}$ and $\mathbf{v}_i^{j+\frac{1}{2}}$ using the Discrete Fourier Transform Method. There are three computing steps.

Step 1. Assuming the initial data: $\alpha_i^0,\theta_i^0,(\alpha_t)_i^0,(\theta_t)_i^0$ are known, we can solve $\alpha_i^1,\theta_i^1,(\alpha_t)_i^{\frac{1}{2}}$ by Eqs. (3.6)-(3.10).

Step 2. Assuming $\alpha_i^j,\alpha_i^{j-1},(\alpha_t)_i^{j-\frac{1}{2}},\theta_i^j,\theta_i^{j-1}$ are known, we can solve θ_i^{j+1} by Eq. (3.4) and $(\alpha_t)_i^{j+\frac{1}{2}}$ by Eqs. (3.11) and (3.13). Then α_i^{j+1} can be resolved. Repeat this step until the time T.

Step 3. By Eqs. (2.28) and (2.29), we obtain the curve **R** and the director field **O**.

For the reduced model, the equations of α are similar, and there is no equation for the director field. Thus, we can use similar numerical discrete equations and algorithms, without needing to solve the equation for θ.

4 Numerical results

We now present some numerical results, which illustrate the various vesicle structures in the 2-dimensional space and the energy landscape. The results also demonstrate clearly that the computing method can achieve the second order accuracy in both time and space. If there is no special explanation, the following values for the parameters will be taken: ϕ=0.001, μ=0.01, ε_1=0.0001, k_1=0.001, k_2=0.002. All the numerical computing programs run on a PC with Pentium(R) IV 3GHz CPU.

4.1 The free membrane

Firstly, we simulate the director model without the osmotic pressure and the spontaneous curvature. As said above, the steady state in this case is just a circle with all directors parallel to the normal vectors. Since there is no energy dissipation in the 2-dimensional space, the curve can not stop moving by itself. Fig. 1 shows the numerical results following the initial state: a rest ellipse, for time T=0.00, T=0.45, T=0.90, T=1.80 respectively.

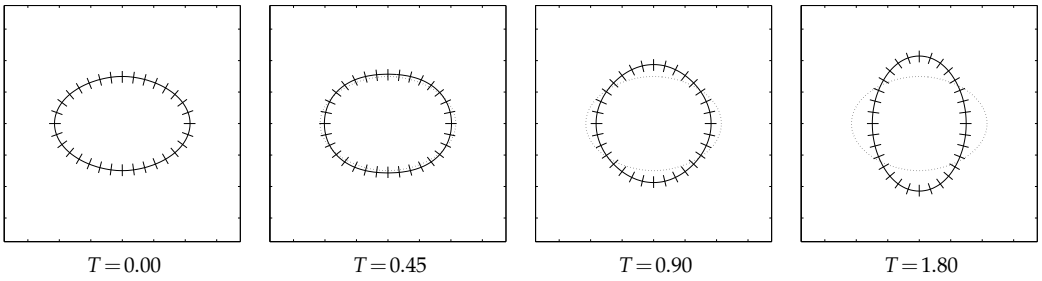

Figure 1: A rest ellipse. The four graphs display the numerical results at the time $T=0.00$, 0.45, 0.90, 1.80 respectively. Dotted curve shows the initial state; solid curve shows the current state; the dashes on the curve are the directors.

In each subgraph, the initial state is displayed as a dotted curve and the current state of the membrane is displayed as the solid curve, on which the dashes are the directors. The graphs in Fig. 2 show the images for the total energy, kinetic energy and elastic energy respectively. In the first image, we subtract 0.01104 from the total energy to study the oscillation. The total energy should be a conservation quantity, and in Fig. 2, the amplitude of its range is about 10^{-6} order of magnitude which can be seen as numerical errors. The graphs show the three kinds of energy all oscillating strongly. Because the length of the director is very short, the directors wiggle fast, causing the numerical oscillation.

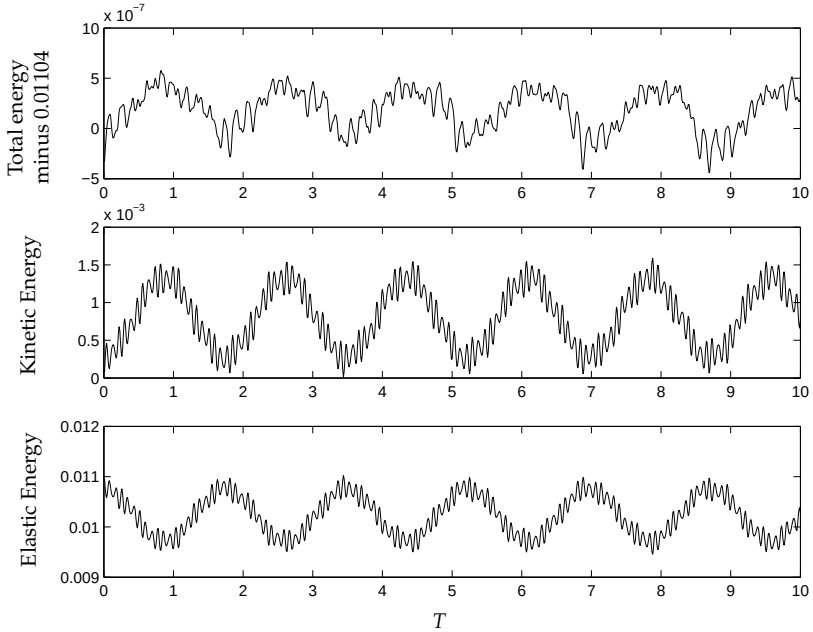

Figure 2: Three energies oscillate strongly, because the directors are so short that they wiggle in a large frequency fast. The total energy should be a conservation quantity. The first graph shows that the amplitude of the total energy's range is about 10^{-6}, which are numerical errors.

Here, we use this numerical experiment to verify the algorithm's second order accuracy in both time and space. We compute the equations with time steps $\Delta t=10^{-3}$, $\frac{1}{2}10^{-3}$,

Table 1: The algorithm's second order accuracy.

Δt	0.001	0.0005	0.00025
$J(\Delta t)$	4.004	4.001	4.000
N	32	64	128
$K(N)$	3.579	3.863	3.972

$\frac{1}{2}10^{-3}$, $\frac{1}{4}10^{-3}$, $\frac{1}{8}10^{-3}$ and the number of discrete points $N=2^6$, 2^7, 2^8, 2^9, 2^{10} from $T=0$ to $T=1$. Denoting the quantity

$$J(\Delta t)=\frac{\left|\left|\mathbf{R}(N,\Delta t)-\mathbf{R}(N,\frac{1}{2}\Delta t)\right|\right|}{\left|\left|\mathbf{R}(N,\frac{1}{2}\Delta t)-\mathbf{R}(N,\frac{1}{4}\Delta t)\right|\right|}$$

with $N=128$, and

$$K(N)=\frac{||\mathbf{R}(N,\Delta t)-\mathbf{R}(2N,\Delta t)||}{||\mathbf{R}(2N,\Delta t)-\mathbf{R}(4N,\Delta t)||}$$

with $\Delta t=10^{-3}$, we obtain the following results (see Table 1). $J(\Delta t)$ and $K(N)$ approximately equal to 4.00. It means the numerical algorithm has second-order accuracy.

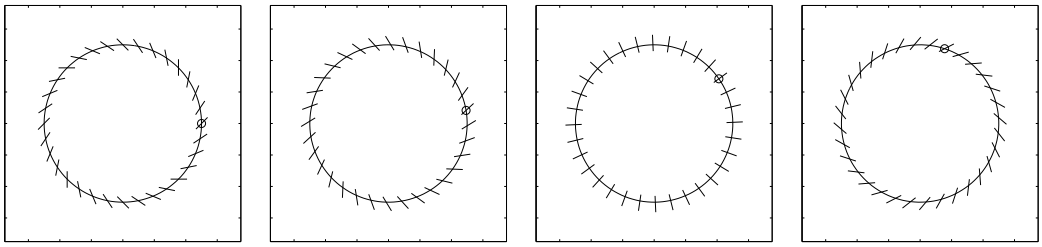

Figure 3: Rest circle with tilted directors. The four graphs show the numerical results at the time $T=0.00$, 0.40, 0.80, 1.60 respectively. At the beginning, there is a tilt angle $\frac{\pi}{4}$ between the director and the normal vector. The directors pull the curve to rotate to make themselves return to the normal directions quickly (from $T=0.0$ to $T=0.80$). Then they wiggle to another side of the normal directions ($T=1.60$) and then move back.

We design a numerical experiment to study the effects of the director field. The initial data is a rest circle and all the directors do not point parallel with the normal vectors. The initial tilt angle between the director and the normal vector is $\frac{\pi}{4}$. We take a large length of the director: $\phi=1.0$, to get a clearer phenomenon. The graphs in Fig. 3 display the numerical results for $T=0.00$, 0.40, 0.80, 1.60. We circle a point to show the rotation of the circle clearer. Since the tilt director tends to return back to the normal direction, the curve is pulled to rotate anticlockwise by the directors ($T=0.40$). While the directors point parallel with the normal directions (T=0.80), the curve has the lowest elastic energy but the largest kinetic energy. The directors go on wiggling to another side of the normal directions ($T=1.60$), and then come back pulling the curve to rotate clockwise. In Fig. 4,

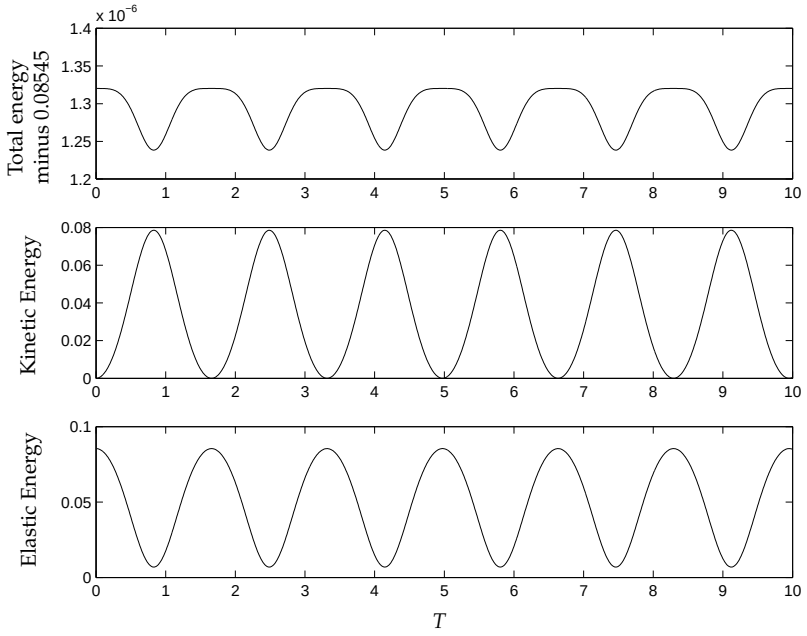

Figure 4: The graphs show the total energy minus 0.08545, kinetic energy and elastic energy respectively. The total energy should be a conservation quantity and the first graph shows that the amplitude of its range is about 10^{-7}, which are numerical errors. These three energies have no strong oscillation which is very different from the process of ellipse (Fig. 4), because the directors are much longer and wiggle in a slow frequency.

the energy does not oscillate strongly, which is different from Fig. 2, because the director is so long that it wiggles in low frequency.

4.2 The effects of the osmotic pressure

Secondly, we simulate the director model with the osmotic pressure. In nature, the cell's volume must be remained in a range. The cell controls its volume by preserving the concentration inside equaling the outside. If the concentrations inside and outside are different, a pressure will push water to permeate through the membrane from the lower-concentration side to the higher side. Based on this point of view, the osmotic pressure $\mathbf{F}_{osm}$ is in direct proportion to the difference between inner and outer concentration, and its direction points parallel with the normal vector

$$\mathbf{F}_{osm} = f_{osm}\mathbf{n} = c_0\left(\frac{1}{V}-\frac{1}{V_0}\right)\mathbf{n},$$

where V and V_0 are the current and balance areas respectively, c_0 is a positive parameter. The osmotic pressure contributes a volume energy to the total energy, and the energy estimation is

$$\frac{\partial}{\partial t}\left[\int_\Gamma\left(\frac{\gamma}{2}|\mathbf{v}|^2+\frac{\gamma\phi}{2}\left|\mathbf{O}\times\frac{\partial\mathbf{O}}{\partial t}\right|^2+E_{el}\right)dS+c_0\left(\frac{V}{V_0}-\ln V\right)\right]=0.$$

The membrane's equilibrium shape minimize the elastic energy plus the volume energy. But the volume term $(V/V_0-\ln V)$ reaches minimum at $V=V_0$, which is not a circle. Thus the structure of the membrane has to balance the elastic energy and the volume energy and the steady state is no longer a circle. Therefore, the osmotic pressure can be considered as constraint of the membrane's inner area, not to leave the area invariable, but to lead the area to the anticipated value. There are some more interesting phenomena.

If the initial state is a rest circle, the osmotic pressure is isotropic at the beginning. But with the accumulation of numerical errors, the osmotic pressure can produce anisotropic effect to make the circle asymmetric. The membrane moves slowly to be concave in two opposite directions and convex in two vertical directions, which looks like a biconcave cell. To accelerate this process, we add a two-periodic initial velocity to the initial conditions:

$$v^1=-\frac{1}{4}\sin(4\pi s),\quad v^{(n)}=\frac{1}{4}\cos(4\pi s),\quad s\in[0,1]. \tag{4.1}$$

The dynamic process is similar with the rest circle initial state. The graphs in Fig. 5 show the numerical results of a circle with two-periodic initial velocity at time $T=0.0$, 0.50, 1.50, 2.60, 3.00, 3.50. While the curve reaches the minimum volume state ($T=1.50$), it will moves back to a biconcave shape in the vertical direction ($T=3.00$, 3.50).

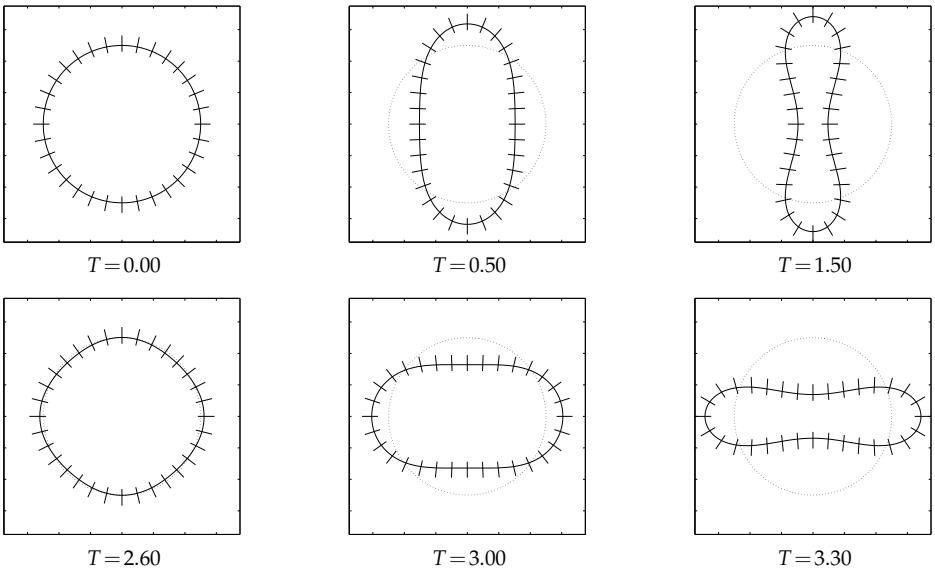

Figure 5: Osmotic pressure: the initial state is a circle with the two-periodic initial velocity (Eq. (4.1)). The first image is the initial circle. By the two periodic velocity, two opposite parts will concave (from $T=0.00$ to $T=1.50$). Since there is no dissipation, the curve will move back ($T=2.60$) and then concave in another two directions ($T=3.00$, 3.30).

If we take three-periodic initial velocity

$$v^1=-\frac{1}{4}\sin(6\pi s),\quad v^{(n)}=\frac{3}{4}\cos(6\pi s),\quad s\in[0,1], \tag{4.2}$$

the circle is concave in three directions and convex in other three opposite directions (see Fig. 6). The curve looks like a triconcave cell (three concave parts).

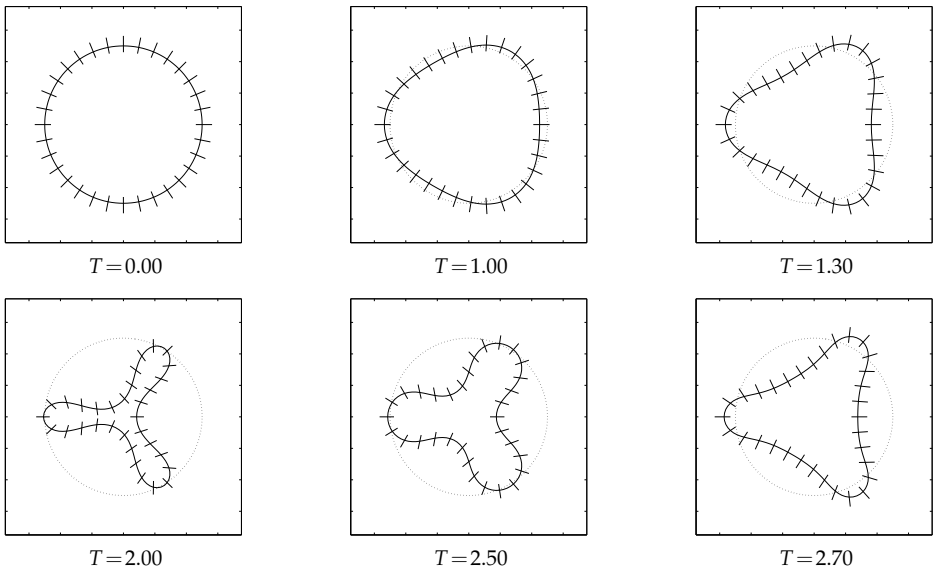

Figure 6: Osmotic pressure: the initial state is a circle with three-periodic initial velocity (Eq. (4.2)). The first graph is the initial circle. By the three periodic velocity, three parts will concave (from $T=0.00$ to $T=2.00$). Since there is no dissipation, the curve will move back ($T=2.50$, 2.70) and then concave in another three directions similar to Fig. 5.

Actually, because the elastic energy of the biconcave steady state is lower than the triconcave state, the dynamic process of the membrane with no initial velocity is biconcave not triconcave. The triconcave state is metastable. The three-periodic initial velocity helps the membrane go beyond the energy barrier.

4.3 The effects of the spontaneous curvature

Thirdly, we consider the effects of the spontaneous curvature. Spontaneous curvature is important for the membrane's shape. The origin of spontaneous curvature is very complex. There are two kinds of explanation. One is about the membrane's bilayer structure. The outer monolayer should have more lipids than the inner one. The difference between the number of two layers causes the spontaneous curvature, which is a global quantity independent of the space. Another one is about the binding of proteins, such as the clatharin coat protein, which support the membrane to keep a certain shape. This property causes the local spontaneous curvature. In the 2-dimensional space, the global spontaneous curvature has no effect. From the Helfrich's curvature elastic energy, we can understand this clearly. The curvature elastic energy in 2-dimensional space is

$$E_H=\int_\Gamma k(\kappa-c_0)^2\,ds=\int_\Gamma k(\kappa^2-2c_0\kappa+c_0^2)\,ds.$$

Since the arc length of the curve and the integral of the curvature on the curve are constants, the global spontaneous curvature has a constant effect on the elastic energy. Thus we only consider local cases. In the director model, the spontaneous curvature is a vector **b** vertical to the director **O**. Here, we set two opposite values to **b**,

$$\begin{cases} \mathbf{b}=7\sin[8\pi(s-\frac{7}{16})](-\sin\theta,\cos\theta), & s\in[\frac{7}{16},\frac{9}{16}], \\ \mathbf{b}=(0,0), & s\in[0,\frac{7}{16})\cup(\frac{9}{16},1), \end{cases} \tag{4.3}$$

and

$$\begin{cases} \mathbf{b}=-7\sin[8\pi(s-\frac{7}{16})](-\sin\theta,\cos\theta), & s\in[\frac{7}{16},\frac{9}{16}], \\ \mathbf{b}=(0,0), & s\in[0,\frac{7}{16})\cup(\frac{9}{16},1). \end{cases} \tag{4.4}$$

The graphs in Figs. 7 and 8 show the numerical results of the director model with the spontaneous curvature given above. Fig. 7 is for (4.3), which is an endocytosis process: the part of the membrane where the spontaneous curvature is positive will concave to form a small bubble in the main body, similar to the white blood cell's phagocytosis. Fig. 8 is for (4.4). It is an exocytosis process: the part which has negative spontaneous curvature will convex to form a small bulb out of the main body, similar to the cell's gemmation.

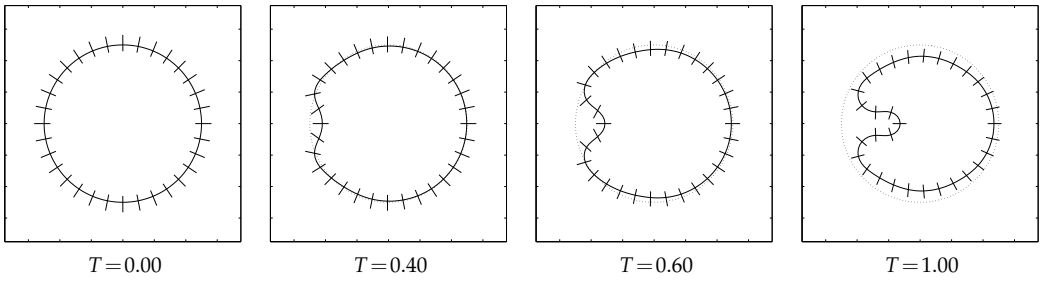

Figure 7: Spontaneous curvature: endocytosis. The directors at the part where the local spontaneous curvature does not vanish will no longer point parallel with each other, but have negative angles. It causes the curve to be concave.

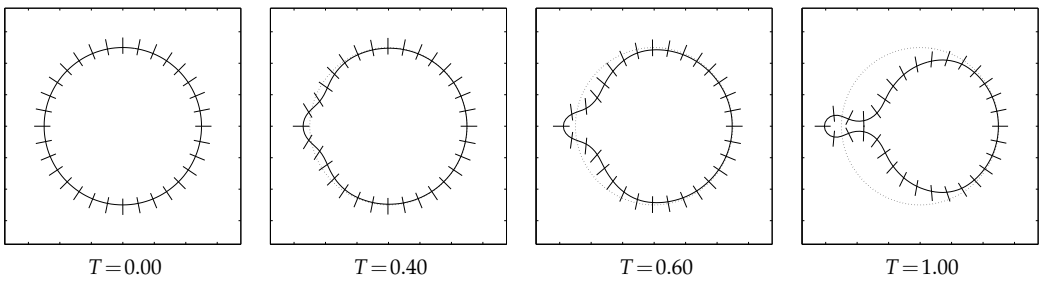

Figure 8: Spontaneous curvature: exocytosis. The directors at the part where the local spontaneous curvature does not vanish will no longer be parallel with neighbors, but have positive angles. It causes the curve to be convex.

4.4 The relation between the director model and the reduced model

The reduced model is a limiting case of the director model. In [1], Hu et al. proved it formally. The reduced model is similar to Waxman's model [9] and they are the same in the 2-dimensional space. We use a similar numerical algorithm to simulate the reduced model.

Table 2 gives the L^2 errors

$$||\mathbf{R}_{director}(T)-\mathbf{R}_{reduced}(T)||_2,$$

which is the error between the director model and the reduced model with different k_2 at time $T=1$. The initial state is a rest circle with three-periodic initial velocity and the directors being parallel with the normal vectors in the director model. From the errors, it is so clearly that as k_2 tending to infinity, the dynamics process of the director model converge to the reduced model. Otherwise, while k_2 tends to infinity, the deflexion of the director **O** from normal position will be smaller and the velocity of director's swing will get larger. The fast wiggling will lead to the shake of the kinetic energy (see Fig. 9).

Table 2: the error $||\mathbf{R}_{director}(T)-\mathbf{R}_{reduced}(T)||_2$ between the director model and the reduced model for different k_2. The initial state is a rest circle with three-periodic velocity. Time is $T=1.0$. As $k_2\to\infty$, the error tends to zero.

k_2	$\|\|\mathbf{R}_{director}(T)-\mathbf{R}_{reduced}(T)\|\|_2$
0.1	2.28583×10^{-1}
0.2	1.37893×10^{-1}
0.4	6.79945×10^{-2}
0.8	3.10456×10^{-2}
1.6	1.29714×10^{-2}
3.2	4.60772×10^{-3}
6.4	2.42708×10^{-3}

5 The director model with area constraint

In nature, the membrane is in a complex environment. There are many things, such as water, protein, lipid, filling around the membrane. These things have a great influence on the membrane's dynamic properties. In this section, we consider the effects of the inner incompressible fluids partially: the area circled by the membrane in the 2-dimensional space is constant. We add the area constraint to the director model, which can describe the dynamics of a curve leaving its local arc length and inner area constant.

5.1 Adding the constraint to the director model

Based on the energy law, physical dynamic processes are optimal in minimizing the total energy. A process remaining a quantity constant means its energy estimation has a La-

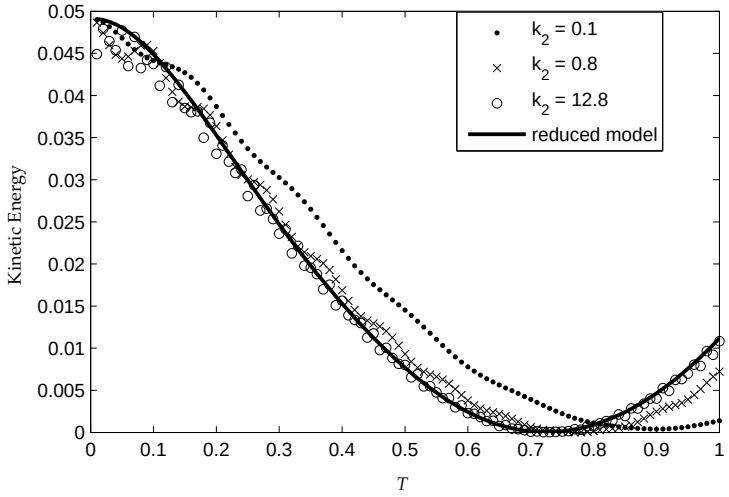

Figure 9: Contrast between the director model and the reduced model. The x-axis is time T, y-axis is the kinetic energy. The solid line is for the reduced model. The dotted line, the dashdot line, and point line are for $k_2=0.1,0.8,12.8$ in the director model respectively. The dynamic process of the director model converges to the reduced model as k_2 tends to infinity.

grangian term to express the constraint. Thus, we add a Lagrangian multiply f_V, which depends only on time but not on space, to the energy estimation to preserve the area:

$$E_{total}=\int_\Gamma\left(\frac{1}{2}\gamma|\mathbf{v}|^2+\frac{1}{2}\left|\mathbf{O}\times\frac{\partial\mathbf{O}}{\partial t}\right|^2+E_{el}\right)ds-f_V(V-V_0). \tag{5.1}$$

Here V_0 and V are the initial and current areas. V can be solved by

$$V=\frac{1}{2}\int_\Gamma\mathbf{R}\cdot\mathbf{n}\,ds. \tag{5.2}$$

By applying the principle of virtual work, we add a "volume force" $f_V\mathbf{n}$ to the director model. Without other extra forces and the spontaneous curvature, the dynamic equations are

$$\gamma\frac{\partial\mathbf{v}}{\partial t}=\frac{\partial(T\mathbf{a})}{\partial s}+k_2\frac{\partial(O^{(n)}O^1\mathbf{n})}{\partial s}+f_V\mathbf{n}, \tag{5.3}$$

$$\gamma\phi\mathbf{O}\times\frac{\partial^2\mathbf{O}}{\partial t^2}=(k_1+\varepsilon_1)\mathbf{O}\times\frac{\partial^2\mathbf{O}}{\partial s^2}-k_2O^1\mathbf{O}\times\mathbf{a}, \tag{5.4}$$

$$\frac{\partial v^1}{\partial s}-\kappa v^{(n)}=0. \tag{5.5}$$

Now, we need another equation for f_V to close the system of equations. The area V remains constant, which means

$$\frac{dV}{dt}=\int_\Gamma v^{(n)}\,ds=0.$$

Taking the time derivative of this equation, we have

$$\frac{d^2V}{dt^2}=\int_\Gamma \frac{\partial v^{(n)}}{\partial t}\,ds=0.$$

Simplifying the middle part

$$\begin{aligned}&\int_\Gamma \frac{\partial v^{(n)}}{\partial t}\,ds=\int_\Gamma \frac{\partial(\mathbf{v}\cdot\mathbf{n})}{\partial t}\,ds\\ &=\int_\Gamma\left(\frac{\partial \mathbf{v}}{\partial t}\cdot\mathbf{n}+\mathbf{v}\cdot\frac{\partial \mathbf{n}}{\partial t}\right)ds\\ &=\int_\Gamma\left[\frac{1}{\gamma}\left(T\kappa+k_2(O^{(n)}O^1)_s+f_V\right)+\mathbf{v}\cdot\frac{\partial \mathbf{n}}{\partial t}\right]ds.\end{aligned}$$

We can get another equation for $T,\mathbf{v},f_V$

$$\frac{d^2V}{dt^2}=Lf_V+\int_\Gamma\left(\frac{1}{\gamma}T\kappa+\mathbf{v}\cdot\frac{\partial \mathbf{n}}{\partial t}\right)ds=0, \tag{5.6}$$

where L is the length of the curve. From this equation, we can express f_V by other variables. But notice that this equation is just a necessary but not a sufficient condition for V to remain constant. Thus, we cannot use this equation alone. We need the condition

$$V=V_0, \tag{5.7}$$

to which we must pay more attention in the numerical simulation. The system of Eqs. (5.3)-(5.7) is the director model with the area constraint.

The term $f_V\mathbf{n}$ looks like the osmotic pressure. They are all the inner area constraint of the membrane, but have different effects. The osmotic pressure comes from the different concentrations between the interior and the exterior of the membrane. It causes the membrane's inner area tend to the expected value. $f_V\mathbf{n}$ comes from the incompressible fluid filling in the membrane. It leaves the membrane's inner area constant.

5.2 Numerical method and results

As in the director model, we introduce the angle α and θ as well, and have the similar equations

$$\gamma\alpha_{tt}=2T_s\alpha_s+T\alpha_{ss}+\frac{1}{2}k_2\left[(\beta_s^2+\alpha_s^2)\sin\beta-\beta_{ss}\cos\beta\right], \tag{5.8}$$

$$-\gamma(\alpha_t)^2=T_{ss}-T(\alpha_s)^2+\frac{1}{2}k_2\left[2\beta_s\alpha_s\cos\beta+\alpha_{ss}\sin\beta\right]+f_V\alpha_s, \tag{5.9}$$

$$\gamma\phi\theta_{tt}=-k_2\cos(\alpha-\theta)\sin(\alpha-\theta)+k\theta_{ss}. \tag{5.10}$$

Eq. (5.6) can be changed into

$$\frac{d^2V}{dt^2}=Lf_V+\int_\Gamma\left(\frac{1}{\gamma}T\alpha_s+\alpha_t v^1\right)ds=0. \tag{5.11}$$

This equation is also a constrained equation for α_t and T. Unfortunately, v^1 cannot be expressed by the angle α directly and only can be solved by

$$\frac{\partial\mathbf{v}}{\partial s}=-\alpha_t\mathbf{n},\quad \int_\Gamma\mathbf{v}\,ds=\int_\Gamma\mathbf{v}_0\,ds,\quad v^1=\mathbf{v}\cdot\mathbf{n},$$

with the periodic boundary condition. We can see that v^1 is dependent on α_t, but it can not be expressed by α_t explicitly.

Taking the same division of the curve Γ and the same symbols, the central differential formulas of Eqs. (5.8)-(5.10) are

$$\gamma\frac{(\alpha_t)_i^{j+\frac{1}{2}}-(\alpha_t)_i^{j-\frac{1}{2}}}{\Delta t}=\left[2T_s\alpha_s+T\alpha_{ss}+\frac{1}{2}k_2\left[(\beta_s^2+\alpha_s^2)\sin\beta-\beta_{ss}\cos\beta\right]\right]_i^j, \tag{5.12}$$

$$-\gamma(\alpha_t)_i^{j+\frac{1}{2}}(\alpha_t)_i^{j-\frac{1}{2}}=\left[T_{ss}-T(\alpha_s)^2+\frac{1}{2}k_2\left[2\beta_s\alpha_s\cos\beta+\alpha_{ss}\sin\beta\right]+f_V\alpha_s\right]_i^j, \tag{5.13}$$

$$\gamma\phi\frac{\theta_i^{j+1}-2\theta_i^j+\theta_i^{j-1}}{\Delta t^2}=\left[-k_2\cos(\alpha-\theta)\sin(\alpha-\theta)+k\theta_{ss}\right]_i^j. \tag{5.14}$$

To get the discrete equation of (5.11), we must notice that Eq. (5.11) is a necessary but not a sufficient condition. In the discrete situation, what we want is to maintain $V^{j+1}=V_0$ by V^j,V^{j-1}. Hence, we can set up the discrete equation

$$\begin{aligned}&\frac{V_0-2V^j+V^{j-1}}{\Delta t^2}\\&=Lf_V^j+\sum_{i=0}^{N-1}\left(\frac{T_i^j}{\gamma}\frac{\alpha_{i+1}^j-\alpha_{i-1}^j}{2\Delta s}+\frac{(\alpha_t)_i^{j+\frac{1}{2}}+(\alpha_t)_i^{j-\frac{1}{2}}}{2}\frac{(v^1)^{j+\frac{1}{2}}+(v^1)_i^{j-\frac{1}{2}}}{2}\right)\Delta s.\end{aligned} \tag{5.15}$$

Putting this equation into Eq. (5.13), we can eliminate f_V^j to get the equations containing only $(\alpha_t)_i^{j+\frac{1}{2}},T_i^j,\theta_i^{j+1}$ (v^1 is dependent upon α_t implicitly) . But in Eq. (5.15) there is a nonlinear term which is a discrete form of $\alpha_t v^1$. We can use the linearized term

$$(\alpha_t)_i^{j+\frac{1}{2}}(v^1)_i^{j-\frac{1}{2}}$$

instead, but it is not a second-order approximation. Thus, we use nonlinear iteration by the steps below to solve the system, with the initial data solved by the linearized formula.

Below we summarize the steps used in our numerical algorithm.

Step 1. We can get the initial data $(\alpha_t)_i^{j+\frac{1}{2},(0)}, T_i^{j,(0)}$ by the linearized equation of Eq. (5.15);

Step 2. Assume we know $(\alpha_t)_i^{j+\frac{1}{2},k}, T_i^{j,k}$, we also have $(v^1)_i^{j+\frac{1}{2},k}$. By the equations

$$\gamma\frac{(\alpha_t)_i^{j+\frac{1}{2},k+1}-(\alpha_t)_i^{j-\frac{1}{2}}}{\Delta t}=\left[2T_s\alpha_s+T\alpha_{ss}+\frac{1}{2}k_2\left[(\beta_s^2+\alpha_s^2)\sin\beta-\beta_{ss}\cos\beta\right]\right]_i^{j,k},$$

$$-\gamma(\alpha_t)_i^{j+\frac{1}{2},k+1}(\alpha_t)_i^{j-\frac{1}{2}}=\left[T_{ss}-T(\alpha_s)^2+\frac{1}{2}k_2[2\beta_s\alpha_s\cos\beta+\alpha_{ss}\sin\beta]+f_V\alpha_s\right]_i^{j,k+1},$$

$$\frac{V_0-2V^j+V^{j-1}}{\Delta t^2}-Lf_V^j=\sum_{i=0}^{N-1}\left(\frac{[T\alpha_s]_i^j}{\gamma}+\frac{(\alpha_t)_i^{j+\frac{1}{2},k}+(\alpha_t)_i^{j-\frac{1}{2}}}{2}\frac{(v^1)^{j+\frac{1}{2},k}+(v^1)_i^{j-\frac{1}{2}}}{2}\right)\Delta s,$$

which is a linear system for $(\alpha_t)_i^{j+\frac{1}{2},(k+1)}$, $T_i^{j,(k+1)}$ and f_V^j, we can solve them. Then repeat Step 2 until convergence.

By these two steps, we can get $(\alpha_t)_i^{j+\frac{1}{2}}$ and T_i^j, and then α_i^{j+1} is obtained. The whole numerical algorithm to solve the area constraint model is similar to the algorithm we used to solve the director model. The difference is that we have to use iteration to solve the quantities in the next time step.

Let $\widetilde{V}$ be the accurate area enclosed by the curve. We use the trapezoidal rule to calculate it. Its error is $\mathcal{O}(\Delta s^2)$ by the periodic boundary condition:

$$\widetilde{V}^{j+1}=\frac{1}{2}\int_\Gamma \mathbf{R}^{j+1}\cdot\mathbf{n}^{j+1}\,ds=V^{j+1}+\mathcal{O}(\Delta s^2), \tag{5.16}$$

$$V^{j+1}=\sum_{i=0}^{n-1}\mathbf{R}_i^{j+1}\cdot\mathbf{n}_i^{j+1}\Delta s. \tag{5.17}$$

Then it is easy to get

$$\begin{aligned}\frac{V^{j+1}-2V^j+V^{j-1}}{\Delta t^2}&=\sum_i(\mathbf{R}_i^{j+1}\cdot\mathbf{n}_i^{j+1}-2\mathbf{R}_i^j\cdot\mathbf{n}_i^j+\mathbf{R}_i^{j-1}\cdot\mathbf{n}_i^{j-1})\frac{\Delta s}{\Delta t^2}\\
&=\frac{\Delta s}{4}\sum_{i=0}^{n-1}\left(\frac{\mathbf{R}_i^{j+1}-2\mathbf{R}_i^j+\mathbf{R}_i^{j-1}}{\Delta t^2}\cdot(\mathbf{n}_i^{j+1}+2\mathbf{n}_i^j+\mathbf{n}_i^{j-1})+\frac{\mathbf{R}_i^{j+1}-\mathbf{R}_i^{j-1}}{2\Delta t}\cdot\frac{\mathbf{n}_i^{j+1}-\mathbf{n}_i^{j-1}}{2\Delta t}\right)\\
&\quad+\frac{1}{4}\sum_{i=0}^{n-1}\left(\mathbf{R}_i^j\cdot(\mathbf{n}_i^{j+1}+\mathbf{n}_i^{j-1})-(\mathbf{R}_i^{j+1}+\mathbf{R}_i^{j-1})\cdot\mathbf{n}_i^j\right)\frac{\Delta s}{\Delta t^2}\\
&=-\sum_i\frac{T_i^j}{\gamma}\frac{\alpha_{i+1}^j-\alpha_{i-1}^j}{2\Delta s}\Delta s+\sum_i(\mathbf{v}^1)_i^j\cdot\frac{(\alpha_t)_i^{j+\frac{1}{2}}+(\alpha_t)_i^{j-\frac{1}{2}}}{2}\Delta s+Lf_V^j+\mathcal{O}(1)\end{aligned} \tag{5.18}$$

by Eq. (5.3). Compared with Eq. (5.15), the numerical error of the accurate area is

$$\widetilde{V}^{j+1} = V_0 + \mathcal{O}(\Delta t^2 + \Delta s^2). \tag{5.19}$$

Here, we use the following curve without velocity and all the directors pointing in normal directions to be the initial state,

$$x = \left(\frac{1}{2} + 0.15\cos\eta\right)\cos\eta,$$
$$y = \left(\frac{1}{3} + \frac{1}{30}\sin\eta\right)\sin\eta,$$

where $\eta \in [0, 2\pi)$ is a parameter. This initial curve looks like an egg (see Fig. 10), whose bigger part is on the left. The motion of this curve is very simple. The bigger part of it will move to right and then move back (see Fig. 11 for time $T=0.00, 0.30, 0.60, 0.90$). From the numerical results, the area V oscillates strongly (see Fig. 12. But the amplitude of its range is only about 3.0×10^{-8}. Our algorithm is found to be powerful in maintaining the area constraint.

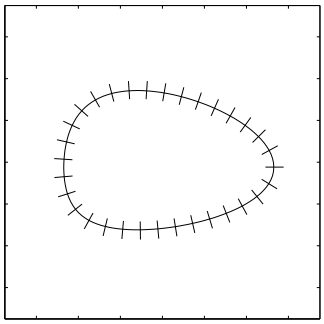

Figure 10: The initial curve, looks like an egg.

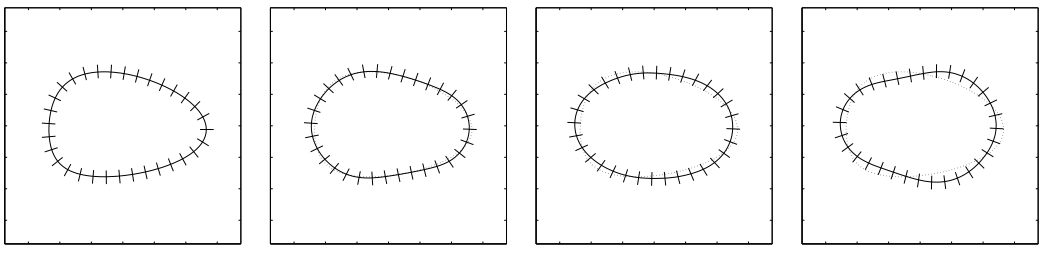

Figure 11: Area constraint. The graphs show the numerical results at time $T=0.00, 0.30, 0.60, 0.90$ respectively. The dotted curve shows the initial state. The bigger part moves to the right and moves back.

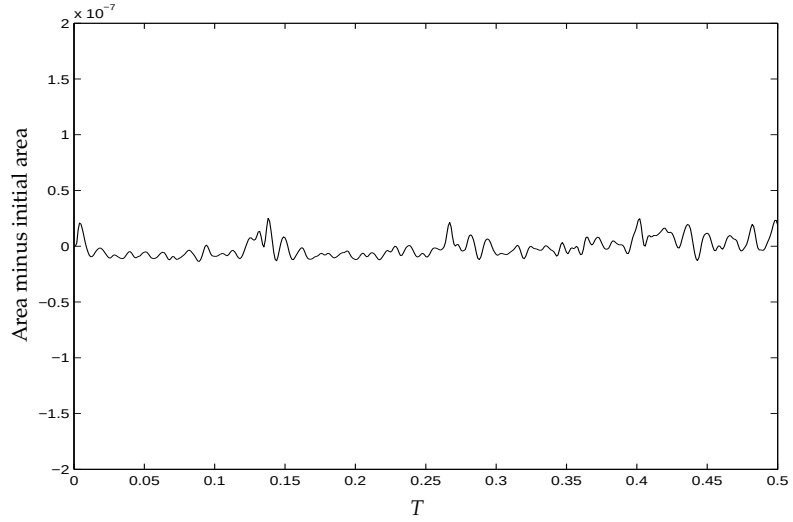

Figure 12: The area minus the initial area. It oscillate strongly, but the amplitude is only 3.0×10^{-8}, which is the numerical error.

6 Conclusion

In this paper, we study the dynamical deformation of a vesicle membrane in the 2-dimensional space by the director model. Several interesting phenomena are discovered from numerical simulations, especially the actions affected by the osmotic pressure and different local spontaneous curvatures. The osmotic pressure can lead the membrane to the shape which circles the anticipant area. With different initial velocities, the membrane has different dynamic processes. The local spontaneous curvature can influence the directors' stable positions and introduce the deformation in some part of the membrane. The vital actions exocytosis and endocytosis are all caused by the local spontaneous curvature. Moreover, by some simulations with different values of the elastic coefficient k_2, the relation between the director model and the reduced model is clear. Finally, considering the incompressible property of the fluid in the membrane partially, we add the inner area constraint to the director model. From the numerical results, we can study the dynamic motion of a membrane whose local arc length and the inner area remain constant.

Acknowledgments

The authors are very grateful to Professors Weinan E and Li-Tien Cheng for their helpful discussions and to Dr. Sharon Murrel for her help in English writing. This work is partially supported by the special funds for Major State Research Projects 2005CB321704 and National Science Foundation of China for Distinguished Young Scholars 10225103 and 20490222.

References

[1] D. Hu, P. Zhang and W. E, The continuum theory of a moving membrane, Phys. Rev. E, 75 (2007), 041605.
[2] W. Helfrich, Elastic properties of lipid bilayers: Theory and possible experiments, Z. Naturforsch. Teil C, 28 (1973), 693-703.
[3] H. J. Deuling and W. Helfrich, The curvature elasticity of fluid membranes: a catalogue of vesicle shapes, J. Physics (France), 37 (1976), 1335-1345.
[4] Z. Ou-Yang and W. Helfrich, Bending energy of vesicle membranes: General expressions for the first, second, and third variation of the shape energy and applications to spheres and cylinders, Phys. Rev. A, 39 (1989), 5280-5288.
[5] D. J. Steigmann, On the relationship between the Cosserat and Kirchhoff-Love theories of elastic shells, Math. Mech. Solids, 4(3) (1999), 275-288.
[6] D. J. Steigmann, Fluid films with curvature elasticity, Arch. Ration. Mech. Anal., 150 (1999), 127-152.
[7] A. M. Waxman, Blood vessel growth as a problem in morphogenesis: A physical theory, Microvasc. Res., 22 (1981), 32-42.
[8] A. M. Waxman, A corotational time derivative for surface tensors, constitutive relations and a new measure of bending strain, J. Non-Newton. Fluid Mech., (1981), 9-235.
[9] A. M. Waxman, Dynamics of a couple-stress fluid membrane, Stud. Appl. Math., 70 (1984), 63-86.
[10] W. Cai and T. C. Lubensky, Hydrodynamics and dynamic fluctuations of fluid membranes, Phys. Rev. E, 53 (1995), 4251-4266.
[11] S. Kwak and C. Pozrikidis, Adaptive triangulation of evolving, closed, or open surfaces by the advancing-front method, J. Comput. Phys., 145 (1998), 61-88.
[12] C. Pozrikidis, Interfacial dynamics for Stokes flow, J. Comput. Phys., 169 (2001), 250-301.
[13] C. Pozrikidis, Modeling and Simulation of Capsules and Biological Cells, CRC Press, 2003.
[14] C. Pozrikidis, Numerical simulation of the flow-induced deformation of red blood cells, Ann. Biomed. Eng., 31(10) (2003), 1194-1205.
[15] C. Pozrikidis, Deformed shapes of axisymmetric capsules enclosed by elastic membranes, J. Eng. Math., 45 (2003), 169-182.
[16] C. Pozrikidis, Resting shape and spontaneous membrane curvature of red blood cells, Math. Med. Biol., 22 (2005), 34-52.
[17] S. Svetina and B. Zeks, Membrane bending energy and shape determination of phospholipid vesicles and red blood cells, Eur. Biophys. J., 17(2) (1989), 101-111.
[18] R. Capovilla and J. Guven, Stresses in lipid membranes, J. Phys. A-Math. Gen., 35 (2002), 6233-6247.
[19] U. Seifert, K. Berndl and R. Lipowsky, Shape transformations of vesicles: Phase diagram for spontaneous-curvature and bilayer-coupling models, Phys. Rev. A, 44 (1991), 1182-1202.
[20] L. Gerald and W. Michael, A numerical study of mechanics of red blood cell shapes and shape transformations, American Physical Society, March Meeting 2004, 2004, pp. 22-26.
[21] Q. Du, C. Liu, R. Ryham and X. Wang, Modeling the spontaneous curvature effects in static cell membrane deformations by a phase field formulation, Commun. Pur. Appl. Anal., 1(4) (2002), 1-12.
[22] Q. Du, C. Liu and X. Wang, A phase field approach in the numerical study of the elastic bending energy for vesicle membranes, J. Comput. Phys., 198 (2004), 450-468.
[23] Q. Du, C. Liu, R. Ryham and X. Wang, A phase field formulation of the Willmore problem,

Nonlinearity, 18 (2005), 1249-1267.
[24] Q. Du, C. Liu and X. Wang, Simulating the deformation of vesicle membranes under elastic bending energy in three dimensions, J. Comput. Phys., 212(2) (2006), 757-777.
[25] E. A. Evans and R. Skalak, Mechanics and Thermodynamics of Biomembranes, CRC Press Boca Raton, 1980.
[26] L. Miao, M. A. Lomholt and J. Kleis, Dynamics of shape fluctuations of quasi-spherical vesicles revisited, Eur. Phys. J. E, 9 (2002), 143-160.
[27] M. A. Lomholt, P. L. Hansen and L. Miao, A general theory of non-equilibrium dynamics of lipid-protein fluid membranes, Eur. Phys. J. E, 16 (2005), 439-461.
[28] M. A. Lomholt and L. Miao, Descriptions of membrane mechanics from microscopic and effective two-dimensional perspectives, J. Phys. A, 39 (2006), 10323-10354.
[29] J. G. Oldroyd, On the formulation of rheological equations of state, Proc. Roy. Soc. Lond. A, 200 (1950), 523-541.
[30] J. G. Oldroyd, The effect of interfacial stabilizing films on the elastic and viscous properties of emulsions, Proc. Roy. Soc. Lond. A, 232 (1955), 567-577.
[31] L. E. Scriven, Dynamics of a fluid interface, Chem. Eng. Sci., 12 (1960), 98-108.
[32] S. May, Y. Kozlovsky, A. Ben-Shaul and M. M. Kozlov, Tilt modulus of a lipid monolayer, Eur. Phys. J. E, 14 (2004), 299-308.
[33] Z. Ou-Yang and W. Helfrich, Bending energy of vesicle membranes:General expressions for the first, second, and third variation of the shape energy and applications to spheres and cylinders, Phys. Rev. A, 39(10) (1989), 5280-5288.
[34] T. S. Sorenson, Dynamics and instability of fluid interfaces, Lect. Notes Phys., 105 (1979), 276-315.
[35] B. W. Macarthur and J. C. Berg, Surface equations of state for insoluble monolayers on aqueous solutions, J. Colloid Interf. Sci., 68 (1979), 201-213.
[36] S. J. Singer and G. L. Nicolson, The fluid mosaic model of the structure of cell membranes, Science, 175 (1972), 720-31.
[37] H. A. Stone, A simple derivation of the time-dependent convective-diffusion equation for surfactant transport along a deforming interface, Phys. Fluids A, 2 (1990), 111-112.
[38] E. M. Toose, B. J. Geruts and J. G. M. Kuerten, A boundary integral method for two-dimensional (non)-Newtonian drops in slow viscous flow, J. Non-Newton. Fluid Mech., 60(2) (1995), 129-154.
[39] R. E. Khayat, Three-dimensional boundary element analysis of drop deformation in confined flow for Newtonian and viscoelastic systems, Int. J. Numer. Meth. Fluids, 34(3) (2000), 241-275.
[40] S. Osher and R. Fedkiw, The Level Set Method and Dynamic Implicit Surfaces, Spinger, Berlin, 2002.
[41] S. Osher and J. Sethian, Fronts propagating with curvature dependent speed: algorithms based on Hamilton Jacobi formulations, J. Comput. Phys., 79 (1988), 12-49.
[42] Y. C. Chang, T. Y. Hou, B. Merriman and S. Osher, Level set formulation of Eulerian interface capturing methods for incompressible fluid flows, J. Comput. Phys., 124(2) (1996), 449-464.
[43] J. Glimm, J. W. Grove, X. L. Li and D. C. Tan, Robust computational algorithms for dynamic interface tracking in three dimensions, SIAM J. Sci. Comput., 21 (2000), 2240-2256.
[44] J. Glimm, X. L. Li, Y. Liu and N. Zhao, Conservative front tracking and level set algorithms, Proceedings of the National Academy of Sciences of the United States of America, 98 (2001), 14198-14201.
[45] T. Y. Hou, J. S. Lowengrub and M. J. Shelley, Removing the stiffness from interfacial flows

with surface tension, J. Comput. Phys., 114 (1994), 312-338.
[46] Q. Nie, The nonlinear evolution of vortex sheets with surface tension in axi-symmetric flows, J. Comput. Phys., 174 (2001), 438-459.
[47] X. Li and Q. Nie, Surface diffusion on stressed solid surface, Commun. Comput. Phys., 2(1) (2007), 73-86.